Factorization and scaling in hadronic diffraction

K. Goulianos and J. Montanha
The Rockefeller University, New York, New York 10021
(Received 16 October 1998; published 6 May 1999)

A comprehensive analysis of single diffraction dissociation data on $p(\bar{p})+p\to p(\bar{p})+X$ from fixed target to collider energies reveals a striking breakdown of factorization, which does not affect the shape of the M_X^2 dependence of the differential cross sections. Phenomenologically, this result can be obtained by postulating a scaling law for hadronic diffraction, which is embedded in the hypothesis of Pomeron flux renormalization introduced to unitarize the triple-Pomeron amplitude. [S0556-2821(99)04111-9]

PACS number(s): 13.85.Ni

I. INTRODUCTION

In Regge theory, the high energy behavior of hadronic cross sections is dominated by Pomeron exchange [1,2]. For a simple Pomeron pole, the pp elastic, total, and single diffractive (SD) cross sections can be written as

$$\frac{d\sigma_{el}}{dt}=\frac{\beta_{\mathbb{P}pp}^4(t)}{16\pi}\left(\frac{s}{s_0}\right)^{2[\alpha_{\mathbb{P}}(t)-1]} \tag{1.1}$$

$$\sigma_T(s)=\beta_{\mathbb{P}pp}^2(0)\left(\frac{s}{s_0}\right)^{\alpha_{\mathbb{P}}(0)-1} \tag{1.2}$$

$$\frac{d^2\sigma_{sd}}{d\xi dt}=\frac{\beta_{\mathbb{P}pp}^2(t)}{16\pi}\xi^{1-2\alpha_{\mathbb{P}}(t)}\left[\beta_{\mathbb{P}pp}(0)g(t)\left(\frac{s'}{s_0}\right)^{\alpha_{\mathbb{P}}(0)-1}\right] \tag{1.3}$$

where $\alpha_{\mathbb{P}}(t)=\alpha_{\mathbb{P}}(0)+\alpha' t=(1+\epsilon)+\alpha' t$ is the Pomeron Regge trajectory, $\beta_{\mathbb{P}pp}(t)$ is the coupling of the Pomeron to the proton, $g(t)$ is the triple-Pomeron coupling, $s'=M^2$ is the $\mathbb{P}-p$ center of mass energy squared, $\xi=1-x_F=s'/s=M^2/s$ is the fraction of the momentum of the proton carried by the Pomeron, and s_0 is an energy scale parameter, which is assumed throughout this paper to be 1 GeV^2 unless appearing explicitly.

In analogy with Eq. (1.2), the term in brackets in Eq. (1.3) is identified as the $\mathbb{P}-p$ total cross section,

$$\sigma_T^{\mathbb{P}p}(s',t)\Rightarrow\sigma_T^{\mathbb{P}p}(s')=\beta_{\mathbb{P}pp}(0)g(0)\left(\frac{s'}{s_0}\right)^{\alpha_{\mathbb{P}}(0)-1}\equiv\sigma_0^{\mathbb{P}p}\left(\frac{s'}{s_0}\right)^{\alpha_{\mathbb{P}}(0)-1} \tag{1.4}$$

where we have used $g(t)=g(0)$, since it was found experimentally that $g(t)$ is independent of t [1]. The remaining factor in Eq. (1.3), namely

$$f_{\mathbb{P}/p}(\xi,t)\equiv\frac{\beta_{\mathbb{P}pp}^2(t)}{16\pi}\xi^{1-2\alpha_{\mathbb{P}}(t)}\equiv K\xi^{1-2\alpha_{\mathbb{P}}(t)}F^2(t) \tag{1.5}$$

where $K\equiv\beta_{\mathbb{P}pp}^2(0)/16\pi$, is interpreted as the ''Pomeron flux.'' Thus, pp diffraction dissociation can be viewed as a process in which Pomerons emitted by one of the protons interact with the other proton [3].

The function $F(t)$ represents the proton form factor, which is obtained from elastic scattering. At small t, $F^2(t)\approx e^{4.6t}$ [4]. However, this simple exponential expression underestimates the cross section at large t. Donnachie and Landshoff proposed [5] that the appropriate form factor for pp elastic and diffractive scattering is the isoscalar form factor measured in electron-nucleon scattering, namely

$$F_1(t)=\frac{4m^2-2.8t}{4m^2-t}\left[\frac{1}{1-t/0.71}\right]^2 \tag{1.6}$$

where m is the mass of the proton. When using this form factor, the Pomeron flux is referred to as the Donnachie-Landshoff (DL) flux.[1] Note that at small-t $F_1^2(t)$ can be approximated with an exponential expression whose slope parameter, $b(t)=(d/dt)\ln F_1^2(t)$, is 4.6 GeV^{-2} at $t\approx-0.04$ GeV^2, consistent with the slope obtained from elastic scattering at small t.

As we discussed in a previous paper [6], the $\sim s^{\epsilon}$ dependence of $\sigma_T(s)$ violates the unitarity based Froissart bound, which states that the total cross section cannot rise faster than $\sim\ln^2 s$. Unitarity is also violated by the s-dependence of the ratio $\sigma_{el}/\sigma_T\sim s^{\epsilon}$, which eventually exceeds the black disc bound of one half ($\sigma_{el}\leq\frac{1}{2}\sigma_T$), as well as by the s-dependence of the integrated diffractive cross section, which increases with s as $\sim s^{2\epsilon}$ and therefore grows faster than the total cross section.

For both the elastic and total cross sections, unitarization can be achieved by eikonalizing the elastic amplitude [6,7], which takes into account rescattering effects. Attempts to introduce rescattering in the diffractive amplitude by including cuts [8,9] or by eikonalization [7] have met with moderate success. Through such efforts, however, it has become clear that these ''shadowing effects'' or ''screening corrections'' affect mainly the normalization of the diffractive amplitude, leaving the form of the M^2 dependence almost unchanged. This feature is clearly present in the data, as demonstrated by the Collider Detector at Fermilab (CDF) Collaboration [10] in comparing their measured diffractive

[1]The factor K in the DL flux is $K_{DL}=(3\beta_{\mathbb{P}qq})^2/4\pi^2$, where $\beta_{\mathbb{P}qq}$ is the Pomeron-quark coupling.

differential $\bar{p}p$ cross sections at $\sqrt{s}=546$ and 1800 GeV with pp cross sections at $\sqrt{s}=20$ GeV.

Motivated by these theoretical results and by the trend observed in the data, a phenomenological approach to unitarization of the diffractive amplitude was proposed [4] based on ''renormalizing'' the Pomeron flux by requiring its integral over all ξ and t to saturate at unity. Such a renormalization, which corresponds to *a maximum* of one Pomeron per proton, leads to interpreting the Pomeron flux as a probability density simply describing the ξ and t distributions of the exchanged Pomeron in a diffractive process (see details in Sec. III).

In this paper, we show that the hypothesis of flux renormalization provides a good description not only of the s-dependence of the total integrated SD cross section, as was already shown in [4], but also of the differential M^2 (or ξ) and t distributions. Specifically, we show that for $M^2>5$ GeV^2 (above the resonance region) and $\xi<0.1$ (the coherence region [1]), all available data for $p+p(\bar{p})\to X+p(\bar{p})$ at small t can be described by a renormalized triple-Pomeron exchange amplitude, plus a non-diffractive contribution from a ''Reggeized'' pion exchange amplitude, whose normalization is fixed at the value determined from charge exchange experiments, $pp\to Xn$. A good fit to the data is obtained using only *one free parameter*, namely the triple-Pomeron coupling, $g(0)$.

We also show that the $t=0$ cross section at small ξ displays a striking scaling behavior, namely $d^2\sigma/dM^2dt|_{t=0}\approx C/(M^2)^{\alpha_{\mathrm{IP}}(0)}$, where the coefficient C is s-independent over six orders of magnitude. In contrast, the $\sim s^{2\epsilon}$ dependence expected from the standard triple-Pomeron amplitude represents an increase of a factor of 6.5 between $\sqrt{s}=20$ and 1800 GeV. This scaling behavior is predicted by the renormalized flux hypothesis and provides a stringent and successful test of its validity.

In Sec. II we present and discuss the data we use in this paper; in Sec. III we describe our phenomenological approach in fitting the data using the Pomeron flux renormalization and pion exchange models; in Sec. IV we present the results of our fits to data; in Sec. V we present the case for a scaling law in diffraction; and in Sec. VI we make some concluding remarks on factorization and scaling in soft diffraction.

II. DATA

The data we use are from fixed target pp experiments [11,12], from CERN Intersecting Storage Rings (ISR) pp experiments [13,14], from CERN Super Proton Synchrotron (S$\bar{p}p$S) Collider $\bar{p}p$ experiments [15], and from $\bar{p}p$ experiments at the Fernilab-Tevatron collider [10,16]. Below, we discuss some aspects of the Tevatron Collider data reported by CDF [10].

A. The CDF data

The CDF Collaboration reported [10] differential cross sections for $\bar{p}p\to\bar{p}X$ in the region of $\xi<0.15$ and $|t|$

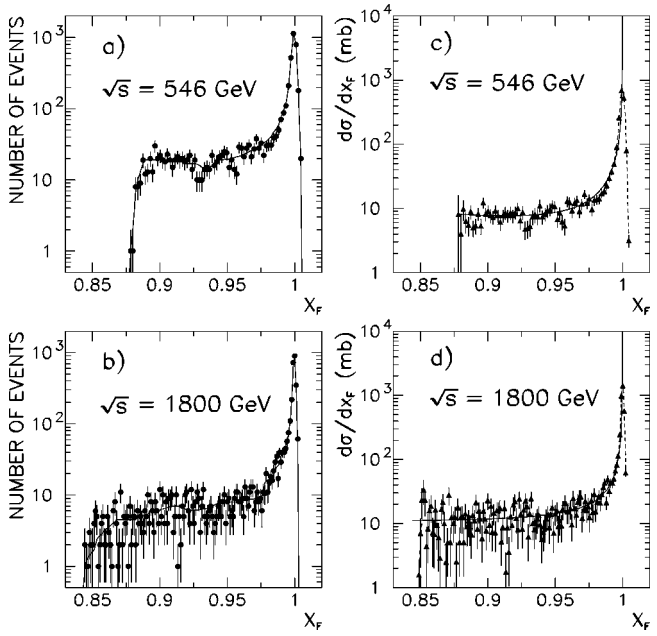

FIG. 1. (a),(b) CDF data for $\bar{p}p\to\bar{p}X$ uncorrected for acceptance (from Ref. [10]): number of events Feynman-x (X_F); the solid line histograms are from a Monte Carlo simulation using formula (2.2); (c),(d) CDF cross sections $d\sigma/dx_F$ (integrated over t); the solid curves represent formula (2.1) and the dashed curves formula (2.2).

$<\sim 0.15$ GeV^2 at $\sqrt{s}=546$ and 1800 GeV. The experiment was performed by measuring the momentum of the recoil antiproton using a roman pot spectrometer. No tables containing data points are given in the CDF publication. The data are presented in two figures (Figs. 13 and 14 in [10]), which are reproduced here as Figs. 1a and 1b, where the number of events is shown as a function of x_F ($x_F=1-\xi$) of the recoil antiproton, rather than as a function of the antiproton momentum (as was done in [10]). The histogram superimposed on the data in each figure is the CDF fit to the data generated by a Monte Carlo (MC) simulation performed by CDF. As an input to the simulation, the following formula was used:

$$\frac{d^2\sigma}{d\xi dt}=\frac{1}{2}\left[\frac{D}{\xi^{1+\epsilon}}e^{(b_0-2\alpha'\ln\xi)t}+I\xi^{\gamma}e^{b't}\right]. \qquad (2.1)$$

The first term in this equation is the triple-Pomeron term of Eq. (1.3). The second term was introduced to account for the non-diffractive background. A connection to Regge theory may be made by observing that $\gamma=1$ ($\gamma=0$) corresponds to pion (Reggeon) exchange with a Regge trajectory of intercept $\alpha(0)=0$ (0.5) (see Sec. III). The factor of $\frac{1}{2}$ does not appear in Ref. [10] and is introduced here to account for the fact that we refer only to the cross section for $\bar{p}p\to\bar{p}X$ and do not include that for $p\bar{p}\to pX$, as was done by CDF. The CDF MC simulation took into account the detector acceptance and the momentum resolution of the spectrometer. The slope of the Pomeron trajectory, α', was kept fixed at the value $\alpha'=0.25$ GeV^{-2}. The values of the remaining param-

TABLE I. CDF fit parameters from Ref. [10].

Parameter	$\sqrt{s}=546$ GeV	$\sqrt{s}=1800$ GeV
D	3.53 ± 0.35	2.54 ± 0.43
b_0	7.7 ± 0.6	4.2 ± 0.5
α'	0.25 ± 0.02	0.25 ± 0.02
ϵ	0.121 ± 0.011	0.103 ± 0.017
I	537^{+498}_{-280}	162^{+160}_{-85}
γ	0.71 ± 0.22	0.1 ± 0.16
b'	10.2 ± 1.5	7.3 ± 1.0
σ_0	1.4×10^{-3}	8.9×10^{-4}

eters, as determined from the CDF fits to the data, are listed in Table I, where we include the values for the momentum resolution, σ_0, at $\sqrt{s}=546$ and 1800 GeV.

1. Acceptance corrected ξ distributions

Using the information provided in the CDF publication, we mapped Figs. 1a and 1b into Figs. 1c and 1d, respectively, in which the data are corrected for detector acceptance. The acceptance was obtained from Fig. 2 of Ref. [10]. The results are presented as cross sections, rather than as events, versus x_F. The normalization was determined by comparing the data points with the CDF MC fits. The number of events corresponding to each x-bin of the MC histograms in Figs. 1a and 1b was converted to an absolute cross section by convoluting the analytic CDF formula for the differential cross section with the t-acceptance function and with the Gaussian ξ-resolution function using a normalization that reproduces the MC histogram. The curves in the new figures represent Eq. (2.1) convoluted with a Gaussian resolution function of ξ, whose width was determined from the momentum resolution of the spectrometer at each energy. Specifically, these curves are calculated using the expression [17,18]

$$\frac{d\sigma}{d\xi}=\int_{t=0}^{-\infty}\frac{d^2\sigma}{d\xi dt}dt;\quad \frac{d^2\sigma}{d\xi dt}=\int_{\xi'=1.4/s}^{1}\frac{d^2\sigma}{d\xi' dt}\;g(\xi',\xi)d\xi' \tag{2.2}$$

where $d^2\sigma/d\xi' dt$ is given by Eq. (2.1) (with $\xi\rightarrow\xi'$) and $g(\xi',\xi)$ is the Gaussian resolution function given by

$$g(\xi',\xi)=\frac{1}{\sqrt{2\pi}\sigma_0}e^{-(\xi'-\xi)^2/2\sigma_0^2}. \tag{2.3}$$

As seen in Figs. 1c and 1d, expression (2.2) provides an excellent fit to the acceptance-corrected differential cross sections, including the unphysical region of negative ξ values. Thus, once the detector experimental resolution is accounted for, the low-ξ (or equivalently, the low-M^2) cross section is *completely compatible* with that expected from extrapolating the cross section from the region of $0.95<x_F<0.99$ ($0.05>\xi>0.01$) into the resolution dominated very low-ξ region using the triple-Pomeron differential cross section shape. This behavior rules out the hypothesis of low-ξ (low-M^2) suppression suggested by some authors [19,20].

TABLE II. Differential cross sections for $pp\rightarrow pX$ as a function of ξ at $|t|=0.05$ GeV^2 [11].

$\sqrt{s}=14$ GeV		$\sqrt{s}=20$ GeV	
ξ	$d^2\sigma/d\xi dt$ (mb/ GeV^2)	ξ	$d^2\sigma/d\xi dt$ (mb/ GeV^2)
0.0160	282.0 ± 11.8	0.0160	233.2 ± 10.9
0.0267	145.6 ± 9.3	0.0267	146.7 ± 7.9
0.0373	112.0 ± 8.4	0.0373	105.9 ± 7.0
0.0480	100.0 ± 7.7	0.0480	78.8 ± 6.2
0.0586	85.8 ± 7.3	0.0586	80.7 ± 6.5
0.0693	79.7 ± 7.1	0.0693	70.2 ± 6.1
0.0800	69.1 ± 7.6	0.0800	57.0 ± 5.8
0.0906	65.4 ± 7.4	0.0906	62.5 ± 6.6
0.1013	51.0 ± 7.5	0.1013	68.6 ± 7.0

2. Cross sections at $t=-0.05$ GeV^2

The CDF data in the triple-Pomeron dominated region of $\xi<0.05$ are concentrated at low t-values, namely $|t|<\sim0.1$ (0.2) GeV^2 for $\sqrt{s}=546$ (1800) GeV (see Fig. 2 of Ref. [10]). Therefore, direct comparison of the CDF data with other experiments should be made for t-values within these regions of t. Since the CDF paper does not report ξ-distributions at a fixed value of t in the form of a table, we extracted such a table for $t=-0.05$ GeV^2 from the information given in the CDF paper. The value of $t=-0.05$ GeV^2 was chosen in order to allow direct comparison of the CDF data with the data of Ref. [11], for which ξ-distributions have been published for $t=-0.05$ GeV^2 and $\sqrt{s}=14$ and 20 GeV (see Table II). The $t=-0.05$ GeV^2 CDF points were evaluated from the data in Figs. 1c and 1d, which represent cross sections integrated over t, by scaling the cross section at each point in ξ by the ratio

$$R(\xi)=\frac{d^2\sigma/d\xi dt|_{t=-0.05}}{d\sigma/d\xi} \tag{2.4}$$

which was calculated using Eq. (2.2). Figures 2a and 2b display the $t=-0.05$ GeV^2 data points grouped into ξ-bins of approximately equal width in a logarithmic scale. Figures 2c and 2d display in a linear ξ-scale the data for $\xi<0.01$, including the unphysical region of negative ξ-values. The horizontal ''error bars'' represent bin widths. The values of the points plotted in Figs. 2a–d are listed in Tables III and IV. The solid (dashed) curves in the figures represent the CDF fits without (with) the convoluted ξ-resolution function, calculated using Eq. (2.1) [Eq. (2.2)]. For $\sqrt{s}=546$ (1800) GeV, the effect of the detector resolution becomes important for $\xi<0.005$ (0.003). Immediately below these values, the data lie higher than the extrapolation of the solid-line fits from the larger ξ-values. This is completely accounted for by the smearing effect of the ξ-resolution, which also accounts for the values of the cross sections in the unphysical negative ξ-regions, as seen in Figs. 2c and 2d. Exact numerical comparisons between data and calculations are presented in Tables III and IV. The entries in these tables labeled ''CDF

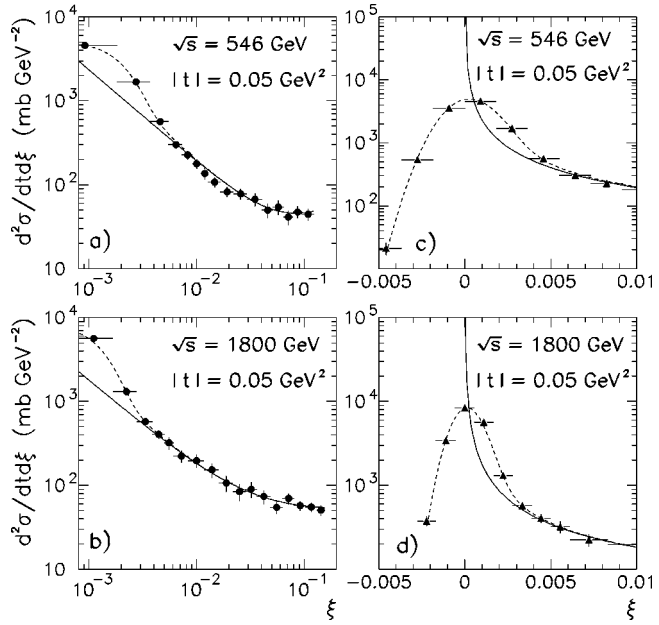

FIG. 2. CDF cross sections $d\sigma/d\xi dt$ at $t=-0.05$ GeV^2; the solid curves represent formula (2.1) and the dashed curves formula (2.2).

fit'' and ''Fit⊗Gauss'' are calculated values of the cross sections per unit ξ and unit t at the center of each bin. The effect of the resolution on the measured cross sections is quite substantial at low-ξ and therefore must be taken into consideration when comparing the low-ξ CDF data with predictions of unitarization models [19,20] based on low-ξ suppression of the diffractive cross section.

TABLE III. Differential cross sections for $\bar{p}p\to\bar{p}X$ at 546 GeV and $|t|=0.05$ GeV^2 extracted from the CDF measurements [10] (see text for details).

ξ	$d^2\sigma/d\xi dt$ (mb/ GeV^2)	CDF fit (mb/GeV^2)	Fit⊗Gauss (mb/GeV^2)
−0.0046	21.18±4.73		16.95
−0.0027	539.1±40.3		569.1
−0.0009	3534.4±124.0		3591.8
0.0009	4561.3±135.1	2568.1	4561.3
0.0027	1682.9±73.8	772.5	1618.2
0.0046	563.0±38.8	443.4	536.2
0.0064	300.9±30.5	308.7	329.0
0.0082	226.5±25.7	236.3	244.8
0.0100	178.2±22.6	191.5	195.9
0.0119	136.5±20.6	161.3	163.9
0.0146	107.3±13.9	131.0	132.3
0.0192	82.4±11.3	101.0	101.6
0.0256	77.9±11.7	78.5	78.8
0.0348	67.0±11.6	62.5	62.6
0.0458	49.6±9.8	53.3	53.3
0.0577	54.4±10.6	48.6	48.6
0.0714	41.2±7.8	46.4	46.4
0.0870	47.7±7.9	45.9	45.9
0.109	44.5±7.1	47.0	47.0

TABLE IV. Differential cross sections for $\bar{p}p\to\bar{p}X$ at 1800 GeV and $|t|=0.05$ GeV^2 extracted from the CDF measurements [10] (see text for details).

ξ	$d^2\sigma/d\xi dt$ (mb/ GeV^2)	CDF fit (mb/GeV^2)	Fit⊗Gauss (mb/GeV^2)
−0.0022	375.4±48.0		307.8
−0.0011	3419.4±182.8		3419.4
0.0000	8368.6±278.9		8368.6
0.0011	5646.9±210.4	1603.4	5019.4
0.0022	1311.9±88.4	776.6	1311.9
0.0033	568.7±66.5	513.7	573.6
0.0044	403.4±57.7	386.1	404.5
0.0055	319.6±52.9	311.3	320.0
0.0072	222.7±35.8	243.7	247.4
0.0100	196.7±33.8	182.9	184.2
0.0139	153.6±29.3	140.1	140.6
0.0189	106.7±22.1	112.1	112.3
0.0250	84.6±18.8	93.8	93.9
0.0322	90.2±18.7	81.6	81.7
0.0422	73.9±13.7	72.2	72.3
0.0555	55.0±9.4	65.3	65.3
0.0717	69.9±10.0	60.8	60.8
0.0918	57.6±7.2	57.8	57.8
0.116	55.4±6.5	55.8	55.8

3. t dependence

We now return to the question of the CDF values of b_0 of the t-distributions (see Table I). Theoretically, the value of b_0 for $\bar{p}p\to\bar{p}X$ should be the same at all energies and equal to one half of the corresponding value for $\bar{p}p\to\bar{p}p$ [see Eqs. (1.1) and (1.3)]. Experimentally, $\frac{1}{2}b_{0,el}=4.6$ GeV^{-2} [4]. The best-fit CDF slope values are $b_0=7.7\pm0.6$ (4.2 ± 0.5) GeV^{-2} for $\sqrt{s}=546$ (1800) GeV. The 1800 GeV value is close to 4.6, within error, but the 546 GeV slope is significantly larger than 4.6 GeV^{-2}. The discrepancy between the slope value measured by CDF at $\sqrt{s}=546$ GeV and the expected value of $b_0=4.6$ GeV^{-2} may be explained by the very short t-range of the experimental measurement. In the region of low-ξ, where Pomeron exchange is dominant, the detector had reasonable acceptance only within the region $0.03<|t|<0.1$ GeV^2. Thus, the slope could not be measured accurately. The quoted error in the measured slope is the standard deviation calculated keeping all other parameters fixed at their best-fit values. The large correlation coefficients [10] between the error of the CDF best-fit parameter b_0 and other fit parameters indicate that a good fit to the data within the t-region of the measurement could have been obtained with a different value of b_0, and correspondingly different value of the other parameters, subject to the constraint that the integrated cross section over the t-range of the measurement remain the same. Since $t=-0.05$ GeV^2 corresponds approximately to the cross-section-weighted mean value of t in the region $0.03<t<0.1$, the value of the differential cross sections at $t=-0.05$ GeV^2 is insensitive to a change in b_0.

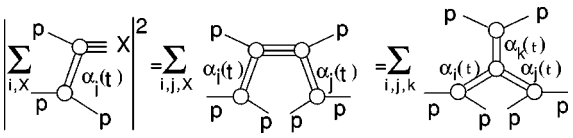

FIG. 3. Illustration of triple-Reggeon phenomenology.

4. Total diffractive cross sections

At $\sqrt{s}=546$ (1800) GeV, the total integrated cross section within the region $0>t>-\infty$ and $(1.5\mathrm{GeV}^2)/s<\xi<0.05$ calculated using Eq. (2.1) (multiplied by a factor of 2 to include the cross section for $\bar{p}p\to Xp$) is 7.28 (8.73) mb.

III. PHENOMENOLOGICAL APPROACH

In the framework of Regge theory [21], the cross section for $pp\to pX$ in the region of large s/M_X^2 can be expressed as a sum of contributions from exchanges of Reggeons i, j and k (see Fig. 3),

$$\frac{d^2\sigma_{sd}}{dM_X^2dt}=\frac{s_0}{s^2}\sum_{i,j,k}G_{ijk}(t)\times\left(\frac{s}{M_X^2}\right)^{\alpha_i(t)+\alpha_j(t)}\left(\frac{M_X^2}{s_0}\right)^{\alpha_k(0)}\cos[\phi_i(t)-\phi_j(t)] \tag{3.1}$$

with

$$G_{ijk}(t)=\frac{1}{16\pi}\beta_{ipp}(t)\beta_{jpp}(t)\beta_{kpp}(0)g_{ijk}(t) \tag{3.2}$$

where $\alpha_i(t)=\alpha_i(0)+\alpha_i't$ is a Reggeon trajectory, β_{ipp} is the Reggeon coupling to the proton, g_{ijk} is the ''triple-Reggeon'' coupling and $\phi_i(t)$ is a phase factor determined by the signature factor, $\eta_i(t)=\zeta+e^{-i\pi\alpha_i(t)}$, where $\zeta=\pm1$ is the signature of the exchange. The signature factors have been expressed as $\eta_i(t)=\eta_i^0(t)e^{i\phi_i(t)}$ with the moduli $\eta_i^0(t)$ absorbed into the $\beta(t)$ parameters in Eq. (3.2). For $pp\to pX$ Reggeons i and j must have the same signature, so that $\phi_i(t)-\phi_j(t)=(\pi/2)[\alpha_i(t)-\alpha_j(t)]$. As mentioned in Sec. I, the energy scale s_0 is not determined by the theory and is usually set to 1 GeV^2. The lack of theoretical input about the value of s_0 introduces an uncertainty in the Pomeron flux normalization, which is resolved in the renormalized Pomeron flux model (see discussion below).

Table V displays the s and ξ, or M_X^2, dependence of the contributions to the $pp\to pX$ cross section at $t=0$ from various combinations of exchanged Reggeons. Three Regge trajectories are considered: the Pomeron, $\mathbb{P}$, with $\alpha_{\mathbb{P}}(0)=1+\epsilon$, the Reggeon, R, with $\alpha_R=0.5$, and the pion, π, with $\alpha_\pi=0$. In fitting elastic and total cross sections, Covolan, Montanha and Goulianos [6] use two Reggeon trajectories, one for the f/a family with $\alpha_{f/a}(0)=0.68$ and the other for the ρ/ω family with $\alpha_{\rho/\omega}(0)=0.46$; Donnachie and Landshoff [2] use one ''effective'' trajectory with $\alpha_R^{eff}(0)=0.55$. For simplicity and clarity of presentation, we consider in Table V one Reggeon trajectory with $\alpha_R(0)=0.5$. The terms $\mathbb{PPP}$ (triple-Pomeron) and $\mathbb{PP}R$ correspond to the picture [3] in which Pomerons emitted by one proton interact with the other proton to produce the diffractive event. The last row in Table V shows the predictions of the renormalized Pomeron flux model [4].

TABLE V. Triple-Reggeon amplitudes for $pp\to pX$ using $\alpha_{\mathbb{P}}(0)=1+\epsilon$, $\alpha_R(0)=0.5$ and $\alpha_\pi(0)=0$.

Amplitude	$d^2\sigma/d\xi dt\vert_{t=0}$	$d^2\sigma/dM^2dt\vert_{t=0}$	$\sigma_{SD}^{tot}(s)$
$(\mathbb{PP})\mathbb{P}$	$\sim\frac{s^\epsilon}{\xi^{1+\epsilon}}$	$\sim\frac{s^{2\epsilon}}{(M^2)^{1+\epsilon}}$	$\sim s^{2\epsilon}$
$(\mathbb{PP})R$	$\sim\frac{1/\sqrt{s}}{\xi^{1.5+2\epsilon}}$	$\sim\frac{s^{2\epsilon}}{(M^2)^{1.5+2\epsilon}}$	$\sim s^{2\epsilon}$
$(RR)\mathbb{P}$	$\sim s^\epsilon\xi^\epsilon$	$\sim\frac{1}{s}(M^2)^\epsilon$	$\sim s^\epsilon$
$(RR)R$	$\sim\frac{1/\sqrt{s}}{\xi^{0.5}}$	$\sim\frac{1/s}{(M^2)^{0.5}}$	$\sim 1/\sqrt{s}$
$(\pi\pi)\mathbb{P}$	$\sim s^\epsilon\xi^{1+\epsilon}$	$\sim\frac{1}{s^2}(M^2)^{1+\epsilon}$	$\sim s^\epsilon$
$(\pi\pi)R$	$\sim(1/\sqrt{s})\xi^{0.5}$	$\sim\frac{1}{s^2}(M^2)^{0.5}$	$\sim 1/\sqrt{s}$
$(\mathbb{P}R)R$	$\sim\frac{1/\sqrt{s}}{\xi^{1+\epsilon}}$	$\sim\frac{s^\epsilon/\sqrt{s}}{(M^2)^{1+\epsilon}}$	$\sim s^\epsilon/\sqrt{s}$
$(\mathbb{P}R)\mathbb{P}$	$\sim\frac{s^\epsilon}{\xi^{0.5}}$	$\sim\frac{s^\epsilon/\sqrt{s}}{(M^2)^{0.5}}$	$\sim s^\epsilon$
Renormalized:			
$(\mathbb{PP})\mathbb{P}$	$\sim\frac{1/s^\epsilon}{\xi^{1+\epsilon}}$	$\sim\frac{1}{(M^2)^{1+\epsilon}}$	$\sim$ constant

A. Standard approach

The standard approach to diffraction is to perform a simultaneous fit to the $pp\to pX$ differential cross sections of all available data at all energies using Eq. (3.1), which is based on factorization. In such a fit, the only free parameters are the triple-Reggeon couplings, $g_{ijk}(t)$. The Reggeon trajectories and the couplings $\beta(t)$ are determined from the elastic and total pp cross sections [6], and the coupling $\beta_{\pi pp}(t)$ is obtained from the coupling $\beta_{\pi np}(t)$, measured in the charge exchange reaction $pp\to nX$, using isotopic spin symmetry: $\beta_{\pi pp}(t)=\frac{1}{2}\beta_{\pi np}(t)$.

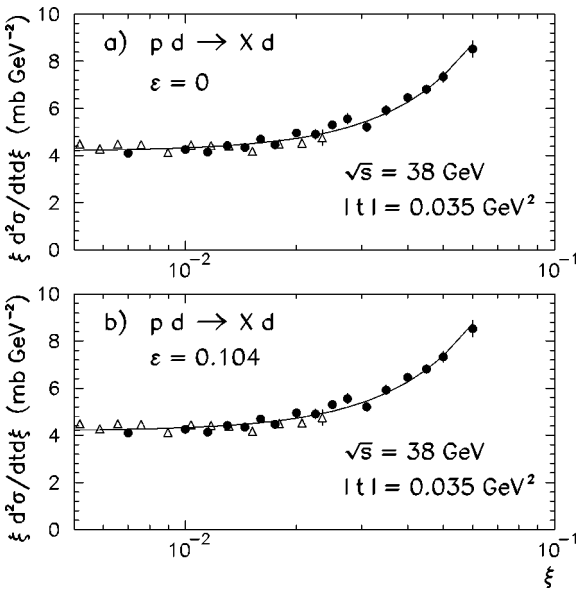

FIG. 4. Cross sections for $p+d\rightarrow X+d$.

1. Factorization

Equation (3.1) is based on factorization. A ''global'' fit of this form to all available data was performed by Field and Fox in 1974 [22]. However, the data available at that time could not constrain the fit well enough to test the triple-Reggeon phenomenology, let alone determine the triple-Reggeon couplings. By 1983, with more data available from Fermilab fixed target and ISR experiments [11–14], good fits to the small-t differential $pp\rightarrow pX$ cross sections were obtained using the empirical expression [1]

$$\frac{d^2\sigma}{d\xi dt}=\frac{A}{\xi}\cdot e^{bt}+B\cdot\xi\cdot e^{b't}. \tag{3.3}$$

The first term in Eq. (3.3) has the ξ-dependence of the $\mathbb{PPP}$ amplitude with $\alpha_{\mathbb{P}}(0)=1$ ($\epsilon=0$) and the second term has the ξ-dependence of the $\pi\pi\mathbb{P}$ amplitude. Note that a Reggeon-exchange contribution, $RR\mathbb{P}$, with $\alpha_R(0)=0.5$, would have a flat ξ-dependence. At the relatively low values of $\sqrt{s}$ of the Fermilab fixed target and ISR experiments, the ξ-range was not large enough for the b-slope to be sensitive to the variation with ξ expected from Eq. (3.1), namely $b=b_0-2\alpha'\ln\xi$, or to distinguish between a $1/\xi$ and a $1/\xi^{1+\epsilon}$ dependence in the first term of Eq. (3.3) and thereby establish the now well known deviation of $\alpha_{\mathbb{P}}(0)$ from unity. Nevertheless, the prominent $\sim 1/\xi$ behavior of the cross section at low-ξ was clear evidence for $\mathbb{PPP}$ dominance and left little room for contributions from other terms, as for example from a $\mathbb{PP}R$ term with its sharper $\sim 1/\xi^{1+0.5}$ dependence on ξ. This is illustrated by the fits of Eq. (3.3) to the very precise data for $pd\rightarrow Xd$ shown in Fig. 4. The data [23,24] are from the experiment of the USA-USSR Collaboration at Fermilab using an internal gas-jet target operated with deuterium. The values of the cross sections at $t=-0.035$ GeV^2 plotted in Fig. 4 were obtained either directly from the published tables [24] or by extrapolation from their published values at $t=-0.05$ GeV^2 [23] using the measured slope of the t-distribution. The two sets of data were normalized to the average value of the cross section within the ξ-region common to both sets of data. Figures 4a and 4b show fits using a $1/\xi$ and a $1/\xi^{1+\epsilon}$ dependence (with $\epsilon=0.104$ [6]), respectively. Both fits are in good agreement with the data.

In summary, the agreement of the Fermilab fixed target and ISR experimental results with the empirical expression (3.3), which is inspired by the factorization based standard triple-Reggeon phenomenology, shows that: (i) at low-ξ, the cross section is dominated by the $\mathbb{PPP}$ amplitude ($\sim 1/\xi$), while (ii) at high-ξ, there is an additional contribution, which has the form of the $\pi\pi\mathbb{P}$ amplitude ($\sim\xi$).

2. Breakdown of factorization

In 1994, when CDF published the diffractive $\bar{p}p\rightarrow\bar{p}X$ cross sections at $\sqrt{s}=546$ and 1800 GeV [10], the supercritical Pomeron trajectory with $\alpha_{\mathbb{P}}(0)>1$ was already well established by fits to total hadronic cross sections [2]. Therefore, CDF made fits using Eq. (2.1), which includes two terms: the $\mathbb{PPP}$ amplitude (first term) and a non-diffractive contribution parametrized as $d^2\sigma_{nd}/d\xi dt=I\xi^{\gamma}e^{b't}$. The form of the latter was inspired by the empirical expression of Eq. (3.3), and the parameter γ was introduced to *effectively* incorporate possible contributions both from $\pi\pi\mathbb{P}$ ($\gamma=1$) and $RR\mathbb{P}$ ($\gamma=0$) amplitudes, as was discussed in Sec. II A.

Three important results from the CDF fits to the data should be emphasized.

Only the $\mathbb{PPP}$ term and a non-diffractive contribution are required by the fits. An upper limit of 15% was set on a possible contribution of a $\mathbb{PP}R$ term to the total diffractive cross section at $\sqrt{s}=546$ GeV. From this result, we derive the following limit for the ratio, R, of the coefficients $G_{ijk}(0)$ of the $\mathbb{PP}R/\mathbb{PPP}$ terms:

$$R\equiv\frac{G_{\mathbb{PP}R}(0)}{G_{\mathbb{PPP}}(0)}<0.2. \tag{3.4}$$

This limit is $\sim 5\%$ of the value of R used in the fit by Erhan and Schlein [20] (see also comments in [25]).

The parameter ϵ was determined for the first time from the ξ-distribution of single diffraction dissociation and was compared to the ϵ obtained from the s-dependence of the total $\bar{p}p$ cross section [26]. The CDF results are:

$$\epsilon(\text{total cross section})=0.112\pm 0.013 \tag{3.5}$$

$$\epsilon(d\sigma/d\xi;\sqrt{s}=546\,\text{GeV})=0.121\pm 0.011 \tag{3.6}$$

$$\epsilon(d\sigma/d\xi;\sqrt{s}=1800\,\text{GeV})=0.103\pm 0.017. \tag{3.7}$$

The values obtained from the $d\sigma/d\xi$ distributions are, within the quoted uncertainties, consistent with the value determined from the rise of the total cross section, as would be expected for Pomeron pole dominance. The weighted average of all three values is [4]

$$\epsilon=0.115\pm 0.008. \tag{3.8}$$

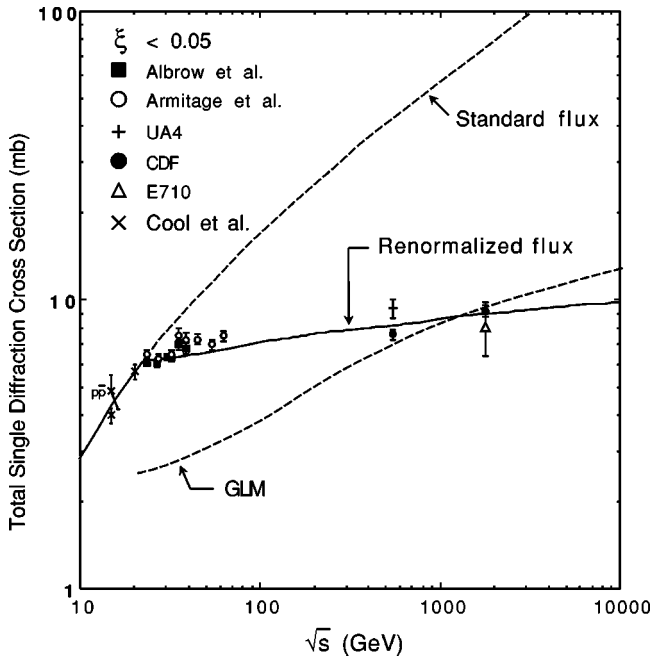

FIG. 5. The total single diffraction cross section for $p(\bar{p})+p \rightarrow p(\bar{p})+X$ versus $\sqrt{s}$ compared with the predictions of the renormalized Pomeron flux model of Goulianos [4] (solid line) and of the model of Gotsman, Levin and Maor [7] (dashed line, labeled GLM); the latter, which includes ''screening corrections,'' is normalized to the average value of the two CDF measurements at $\sqrt{s}=546$ and 1800 GeV.

Using the relation $\xi=M^2/s$, the $\mathbb{PPP}$ (first) term in Eq. (2.1) can be written in terms of M^2 as [see also Eq. (3.1)]

$$\frac{d^2\sigma}{dM^2dt}=\frac{G(0)}{2}(s/s_0)^{\delta}\frac{s_0^{\epsilon}}{(M^2)^{1+\epsilon}}e^{(b_0+2\alpha'\ln(s/M^2))t} \tag{3.9}$$

where in standard Regge theory $\delta=2\epsilon$. Treating δ as a free parameter and performing a simultaneous fit to the diffractive cross sections, σ_{sd}, at $\sqrt{s}=20$ [11], 546 and 1800 GeV, CDF obtained $\delta=0.030\pm0.016$.

The last result indicates a breakdown of factorization. The observed slower than $\sim(s/s_0)^{2\epsilon}$ increase of the diffractive cross section with energy is necessary to preserve unitarity and was predicted in 1986 [8] by calculations including shadowing effects from multiple Pomeron exchanges. More recent work based on eikonalization of the diffractive amplitude [7] or on the inclusion of cuts [9] shows that shadowing can produce substantial damping of the s-dependence of the cross section but has no appreciable effect on the M^2-dependence. These predictions are in general agreement with the conclusions reached by the CDF fits to data. However, the damping predicted by the eikonalization model is not sufficient to account for the observed s-dependence of the total single diffraction cross section (see Fig. 5); the predictions of the model based on cuts are in better agreement with the data [9].

B. Renormalized Pomeron flux approach

1. Triple-Pomeron renormalization

The CDF measurements showed that, just like at Fermilab fixed target and ISR energies, the shape of the low-M^2 (low-ξ) behavior of the diffractive cross section at the Tevatron Collider is described well by the $\mathbb{PPP}$ amplitude displayed in Eq. (3.9). The total diffractive cross section, obtained by integrating Eq. (3.9) over all t and over M^2 from $M^2_{min}=1.5$ GeV^2 to $M^2_{\max}=0.1s$, increases with s as $\sim(s/s_0)^{\delta}$. For $\delta=2\epsilon$, which is the value for simple pole exchange, σ_{sd} would increase faster than the total $\bar{p}p$ cross section, which varies as $\sim(s/s_0)^{\epsilon}$, leading to violation of unitarity. With the experimentally determined value of $\delta\approx0$, the diffractive cross section remains safely below the total cross section as s increases, preserving unitarity.

As discussed in the previous section, introducing shadowing corrections can dampen the increase of the diffractive cross section with s and thereby achieve the desired unitarization while preserving the M^2-dependence of the $\mathbb{PPP}$ amplitude, as required by the data. However, the shadowing models do not account completely for the s-dependence of the data, and the two models mentioned above do not predict the same amount of s-damping of the cross section. In addition, these models are very cumbersome to use in calculations of single diffraction, double diffraction and double-Pomeron exchange processes.

The calculational difficulties of unitarity corrections in the standard approach are overcome in the ''Pomeron flux renormalization'' approach proposed by Goulianos [4]. The renormalized flux approach is based on a *hypothesis*, rather than on an actual calculation of unitarity corrections, and therefore can be stated as an axiom.

The Pomeron flux integrated over all phase space saturates at unity.

The standard Pomeron flux is displayed in Eq. (1.5). Using $F^2(t)=e^{b_0t}$, the integral of the standard flux,

$$N(s)=\int_{\xi_{\min}}^{\xi_{\max}}\int_{-\infty}^{0}f_{\mathbb{P}/p}(\xi,t)d\xi dt, \tag{3.10}$$

is given by

$$N(s)=K\frac{e^{-r}}{2\alpha'}[E_i(r-2\epsilon\ln\xi_{\min})-E_i(r-2\epsilon\ln\xi_{\max})] \tag{3.11}$$

where $Ei(x)$ is the exponential integral function,[2] $r\equiv b_0\epsilon/\alpha'$, $\xi_{\min}=M_0^2/s=1.5/s$ is the effective diffractive threshold, and $\xi_{\max}=0.1$ [4].

The renormalized Pomeron flux, $f_N(\xi,t)$, can now be expressed in terms of the standard flux, $f_{\mathbb{P}/p}(\xi,t)$, as follows:[3]

[2] $E_i(x)=\gamma+\ln x+\Sigma_{n=1}^{\infty}(x^n/nn!)$, where $\gamma=0.57721\ldots$ (Euler's constant).

[3] For a detailed discussion of the role of the scale parameter s_0 in determining the value of s for which $N(s)=1$ see [4].

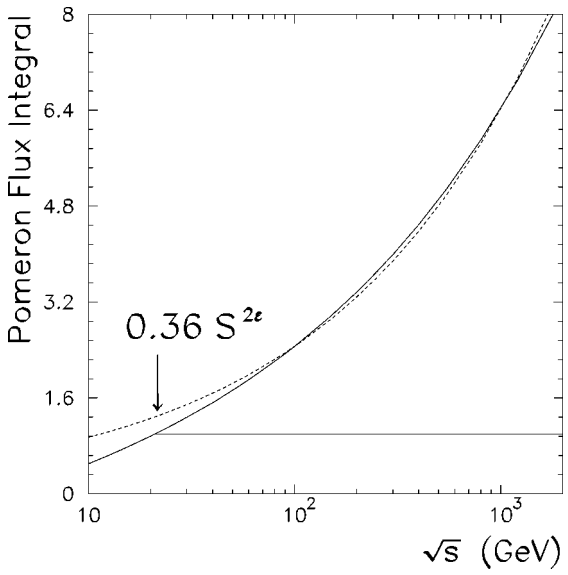

FIG. 6. The integral of the standard Pomeron flux for $pp \to pX$, $N(s)$ of Eq. (3.10) using $F^2(t)=e^{4.6t}$, as a function of $\sqrt{s}$ (solid curve) is compared with a dependence $\sim s^{2\epsilon}$ (dashed curve). The horizontal solid line at $N(s)=1$ represents the *saturated* renormalized flux. If the flux integral is calculated using in Eq. (3.10) the $F_1(t)$ form factor of Eq. (1.6), it can be approximated by the expression $0.41s^{2\epsilon}$.

$$f_N(\xi,t)=\begin{cases} f_{\mathbb{P}/p}(\xi,t) & \text{if } N(s)<1, \\ N^{-1}(s) f_{\mathbb{P}/p}(\xi,t) & \text{if } N(s)>1. \end{cases} \tag{3.12}$$

The renormalized $\mathbb{PPP}$ contribution to the differential cross section is given by

$$\frac{d^2\sigma_{sd}}{d\xi dt}=\frac{K}{N(s)}\,\frac{e^{-2\alpha' t\ln\xi}F^2(t)}{\xi^{1+2\epsilon}}\,\sigma_0^{\mathbb{P}p}(s\xi)^{\epsilon} \tag{3.13}$$

or, in terms of M^2, by

$$\frac{d^2\sigma_{sd}}{dM^2dt}=\frac{Ks^{2\epsilon}}{N(s)}\,\frac{e^{-2\alpha' t\ln(M^2/s)}F^2(t)}{(M^2)^{1+2\epsilon}}\,\sigma_0^{\mathbb{P}p}(M^2)^{\epsilon}. \tag{3.14}$$

In the energy interval of $\sqrt{s}=20$ to 2000 GeV, the standard flux integral varies as $\sim s^{2\epsilon}$ (see Fig. 6). Thus, flux renormalization approximately cancels the s-dependence in Eq. (3.14), resulting in a slowly rising total diffractive cross section. Asymptotically, as $s\to\infty$, the renormalized total diffractive cross section reaches a constant value:

$$\lim_{s\to\infty}\sigma_{sd}^N(s)=\lim_{s\to\infty}\frac{\sigma_{sd}(s)}{N(s)}=2\sigma_0^{\mathbb{P}p}e^{r/2}. \tag{3.15}$$

The s-dependence of the integral of expression (3.13) over all t and $\xi<0.05$, multiplied by a factor of 2 to account for both $\bar{p}p\to\bar{p}X$ and $\bar{p}p\to Xp$, is compared with experimental data for $\sigma_{sd}(\xi<0.05)$ in Fig. 5 (from [4]). In view of the systematic uncertainties in the normalization of different sets of data, which are of $\mathcal{O}(10\%)$, the agreement is excellent.

2. Pion exchange contribution

The form of the empirical expression (3.3) suggests that at high-ξ the dominant non-$\mathbb{PPP}$ concontribution to the cross section comes from pion exchange. In Regge theory, the pion exchange contribution has the form

$$\frac{d^2\sigma}{d\xi dt}=f_{\pi/p}(\xi,t)\sigma^{\pi p}(s\xi) \tag{3.16}$$

where $f_{\pi/p}(\xi,t)$ is the pion flux and $\sigma^{\pi p}(s\xi)$ the πp total cross section.

In the ''Reggeized'' one-pion-exchange model [22], the pion flux is given by

$$f_{\pi/p}(\xi,t)=\frac{1}{4\pi}\,\frac{g_{\pi pp}^2}{4\pi}\,\frac{|t|}{(t-m_\pi^2)^2}\,G_1^2(t)\,\xi^{1-2\alpha_\pi(t)} \tag{3.17}$$

where $g_{\pi pp}^2/4\pi\approx 14.6$ [22] is the on mass-shell coupling, $\alpha_\pi(t)=0.9t$ is the pion trajectory, and $G_1^2(t)$ is a form factor introduced to account for off mass-shell corrections. For $G_1(t)$ we use the expression (see [27] and references therein)

$$G_1(t)=\frac{2.3-m_\pi^2}{2.3-t}. \tag{3.18}$$

Since the exchanged pion is not far off-mass-shell, we use the on-shell πp total cross section [6],

$$\begin{aligned}\sigma^{\pi p}(mb)&=\frac{1}{2}(\sigma^{\pi^+ p}+\sigma^{\pi^- p}) \\ &=10.83(s\xi)^{0.104}+27.13(s\xi)^{-0.32}.\end{aligned} \tag{3.19}$$

3. A one parameter fit to diffraction

Motivated by the success of the empirical expression (3.3) in describing the Fermilab fixed target and ISR data, and by the similarity between this expression and the CDF fits to data at Tevatron energies, we have performed a simultaneous fit to single diffraction differential cross sections at all energies using the formula

$$\frac{d^2\sigma}{d\xi dt}=f_N(\xi,t)\sigma^{\mathbb{P}p}(s\xi)+f_{\pi/p}(\xi,t)\sigma^{\pi p}(s\xi) \tag{3.20}$$

in which the first term is the renormalized triple-Pomeron amplitude, Eq. (3.13), and the second term is the pion exchange contribution, Eq. (3.16). Results from our fit, in which only the triple-Pomeron coupling, $g_{\mathbb{PPP}}$, is treated as a free parameter, are presented in the next section.

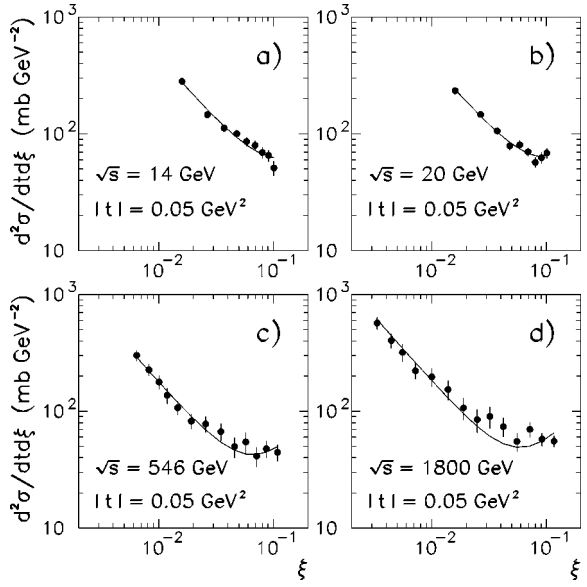

FIG. 7. Cross sections $d^2\sigma_{sd}/d\xi dt$ for $p+p(\bar{p})\to p(\bar{p})+X$ at $t=-0.05$ GeV^2 and $\sqrt{s}=14$, 20, 546 and 1800 GeV. The solid lines represent the best fit to the data at each energy using two terms, the $\mathbb{PPP}$ and $\pi\pi\mathbb{P}$ amplitudes, with their normalizations treated as free parameters.

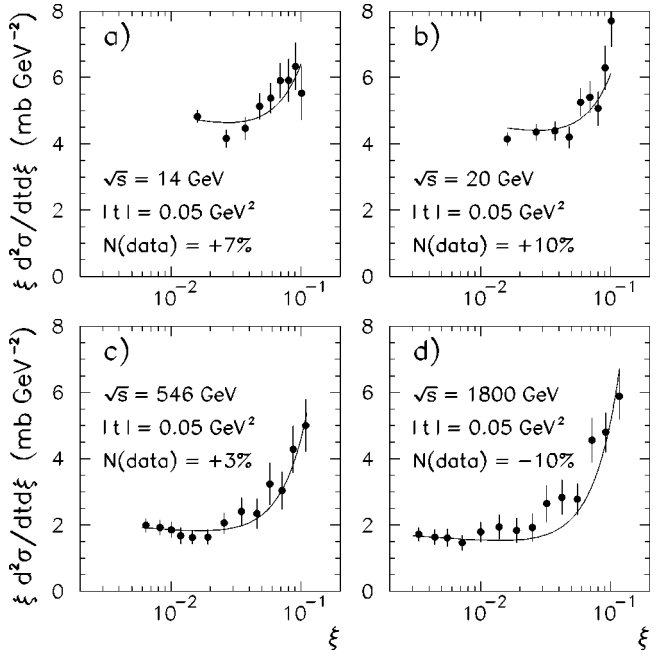

FIG. 8. Cross sections $\xi\cdot d^2\sigma_{sd}/d\xi dt$ for $p+p(\bar{p})\to p(\bar{p})+X$ at $t=-0.05$ GeV^2 and $\sqrt{s}=14$, 20, 546 and 1800 GeV are compared with the results (solid lines) of a simultaneous one parameter fit using a renormalized $\mathbb{PPP}$ amplitude and a Reggeized pion exchange contribution. To account for systematic uncertainties, the normalization of each data set was allowed to vary within $\pm 10\%$ of its nominal value; the parameter ''N(data)'' represents the shift in the data normalization for which the best fit was obtained.

IV. RESULTS

In this section, we present the results of fits performed to experimental data using Eq. (3.20), which has two contributions: a renormalized triple-Pomeron amplitude and a Reggeized pion exchange term.

A. Differential cross sections

The experimental ξ-distributions are usually distorted in the low-ξ region by the resolution in the measurement of the momentum of the recoil $p(\bar{p})$. We therefore check first how well Eq. (3.20) reproduces the shapes of the differential cross sections of the pp data of E396 [11] at $\sqrt{s}=14$ and 20 GeV and of the $\bar{p}p$ data of CDF [10] at $\sqrt{s}=546$ and 1800 GeV in the regions of ξ not affected by detector resolution. Figure 7 shows the cross sections $d^2\sigma_{sd}/d\xi dt$ at $t=-0.05$ GeV^2 for E396 and CDF (data from Tables II, III and IV). The solid lines represent the best fit to the data at each energy using Eq. (3.20) with the normalizations of the triple-Pomeron and pion exchange contributions treated as free parameters. The quality of these fits indicates that no Reggeon terms other than the triple-Pomeron and pion exchange terms are needed to describe the shapes of the differential ξ-distributions.

Figures 8 and 9 show the result of a simultaneous fit (solid lines) to the $t=-0.05$ GeV^2 data of E396 and CDF using Eq. (3.20) with only the triple-Pomeron coupling as a free parameter. The overall normalization of the data was allowed to vary within $\pm 10\%$ to account for possible systematic effects in the experimental measurements. The shift in the normalization of the data at each energy that resulted in the best fit is given in each plot. In Fig. 9 the individual contributions of the triple-Pomeron and pion exchange terms are shown by dashed curves. The fit has a $\chi^2=1.0$ per degree of freedom.

The parameters used in the fit are $\alpha_{\mathbb{P}}(t)=1.104+0.25t$ and $\beta_{\mathbb{P}pp}(0)=6.57$ GeV^{-1} (4.1 mb$^{1/2}$) for the triple-Pomeron term, and those given in Sec. III B 2 for the pion exchange term. The fit yielded a triple-Pomeron coupling $g_{\mathbb{PPP}}=1.0$ GeV^{-1}(0.62 mb$^{1/2}$), which corresponds to $\sigma_0^{\mathbb{P}p}=2.6$ mb; using the $F_1(t)$ form factor yields $g_{\mathbb{PPP}}=1.1$ GeV^{-1} (0.69 mb$^{1/2}$) and $\sigma_0^{\mathbb{P}p}=2.8$ mb.

Figure 10 shows a fit of Eq. (3.20) to ISR data [13] of $d\sigma/d\xi dt$ versus ξ at fixed t. In this fit, the experimental ξ-resolution was taken into account by convoluting Eq. (3.20) with the Gaussian resolution function, Eq. (2.3), using $\sigma_0=0.003$. The parameters used in Eq. (3.20) were those of the above fit to the $p(\bar{p})$ data. The overall normalization of the data has an experimental systematic uncertainty of 15% [13].

B. Total diffractive cross sections

In Fig. 11, we compare experimental results for the total diffractive cross section within $0\leqslant -t\leqslant -\infty$ and $\xi=M_X^2/s\leqslant 0.05$ with the cross section calculated from the triple-Pomeron term of Eq. (3.20) (solid line) using the triple-Pomeron coupling evaluated from the fit to the differential cross sections. Within this region of ξ, the expected contri-

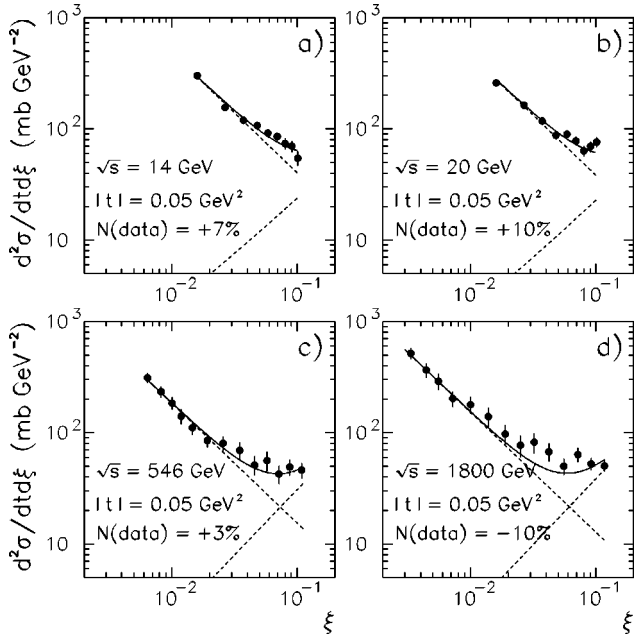

FIG. 9. Cross sections $d^2\sigma_{sd}/d\xi dt$ for $p+p(\bar{p})\rightarrow p(\bar{p})+X$ at $t=-0.05$ GeV^2 and $\sqrt{s}=14$, 20, 546 and 1800 GeV are compared with the results (solid lines) of a simultaneous one parameter fit with a renormalized PPP amplitude and a pion exchange contribution. The dashed lines represent the individual Pomeron and pion contributions. To account for systematic uncertainties, the normalization of each data set was allowed to vary within $\pm 10\%$ of its nominal value; the parameter ''N(data)'' represents the shift in the data normalization for which the best fit was obtained.

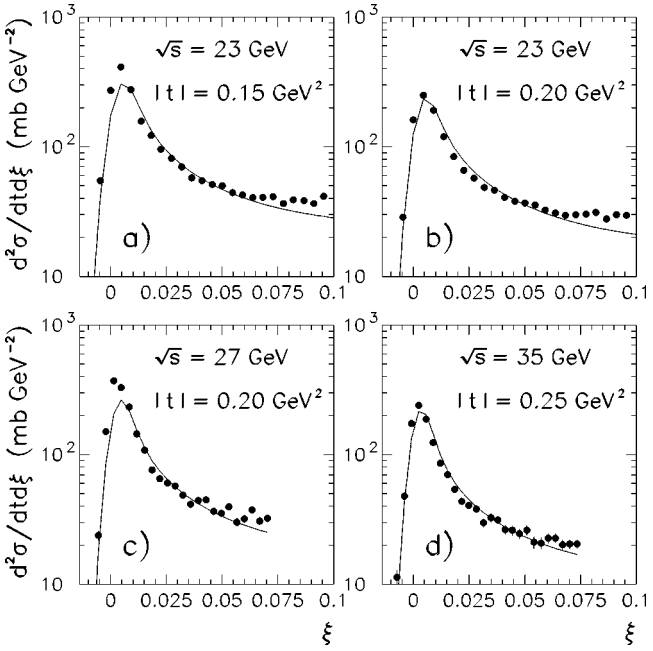

FIG. 10. Cross sections $d^2\sigma_{sd}/d\xi dt$ for $pp\rightarrow pX$ measured at the ISR at various values of $\sqrt{s}$ and t, as indicated in each plot. The solid lines are fits obtained using the renormalized PPP amplitude and the pion exchange contribution, convoluted with the experimental ξ resolution, which dominates the shape of the distributions at small ξ. The overall normalization of the data has a systematic uncertainty of $\pm 15\%$ [13].

bution of the pion exchange term is less than 2% at any given energy. The data points are from Refs. [10–16].

There are two points that must be kept in mind in comparing data with theory.

(a) *Normalization of data sets.* The *overall* normalization uncertainty in each experiment is of $\mathcal{O}(10\%)$.

(b) *Corrections applied to data.* Deriving the total cross section from experimental data invariably involves extrapolations in t and ξ from the regions of the measurement to regions where no data exist. In making such extrapolations, certain assumptions are made about the shape of the t-distribution and/or the shape of the ξ distribution. With the exception of the ISR experiments [13,14], all measurements of the experiments listed here are at very low-t. In these cases, an exponential form factor of the form $e^{b_0 t}$ was assumed for extrapolating into the high-t region. The (higher-t) ISR data show a clear deviation from exponential behavior and support the $F_1^2(t)$ form factor. Using $F_1^2(t)$ instead of $e^{b_0 t}$ results in a *larger* total cross section by $\sim 5-10\%$, depending on the value of s (smaller correction at higher s). The magnitude of the correction depends on the ξ-region and, through ξ, on s, since the t-distribution depends not only on the form factor but also on ξ through the term $e^{(-2\alpha' \ln\xi)t}$.

Another source of error comes from the fact that the slope of the t-distribution is usually not measured accurately in experiments sensitive only to low-t. The discussion in Sec. II A 3 of the CDF measurement at $\sqrt{s}=546$ GeV illustrates this point.

Table VI presents the total diffractive cross sections corrected for the effects mentioned above. The ISR [13,14] and $S\bar{p}pS$ [15] cross sections were left unchanged, since they

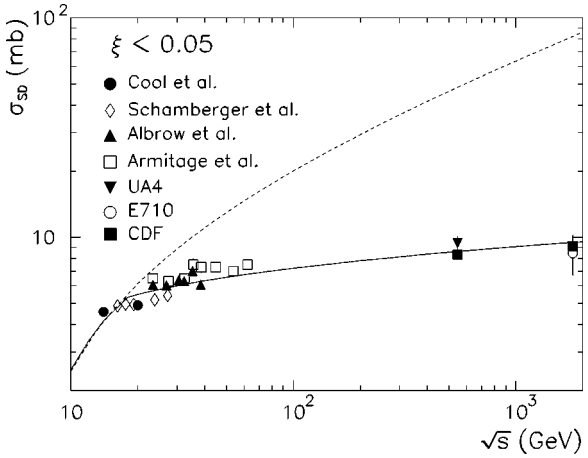

FIG. 11. Total single diffraction cross sections for $p(\bar{p})+p\rightarrow p(\bar{p})+X$ versus $\sqrt{s}$ compared with triple-Pomeron predictions based (a) on Pomeron pole dominance in standard Regge theory (dashed line) and (b) on the renormalized Pomeron flux model [4] (solid line). The cross sections were corrected for effects due to extrapolations in t, as discussed in the text. The errors shown are statistical; typical systematic uncertainties for each experiment are of $\mathcal{O}(10\%)$.

TABLE VI. Total $p/\bar{p}\to p/\bar{p}X$ single diffraction cross sections for $\xi\leqslant 0.05$ (includes both interacting hadrons). The cross sections of the references marked with † were derived from the experimental data using the procedure outlined in the text.

$\sqrt{s}$ (GeV)	σ_{sd} (mb)	Ref.	$\sqrt{s}$ (GeV)	σ_{sd} (mb)	Ref.
14	3.94 ± 0.20	† [11]	23.3	6.5 ± 0.2	[14]
20	4.46 ± 0.25	† [11]	27.4	6.3 ± 0.2	[14]
16.2	4.87 ± 0.08	† [12]	32.4	6.5 ± 0.2	[14]
17.6	4.96 ± 0.08	† [12]	35.5	7.5 ± 0.5	[14]
19.1	4.94 ± 0.08	† [12]	38.5	7.3 ± 0.4	[14]
23.8	5.19 ± 0.08	† [12]	44.7	7.3 ± 0.3	[14]
27.2	5.42 ± 0.09	† [12]	53.7	7.0 ± 0.3	[14]
23.4	6.07 ± 0.17	[13]	62.3	7.5 ± 0.3	[14]
26.9	6.05 ± 0.22	[13]	546	9.4 ± 0.7	[15]
30.5	6.37 ± 0.15	[13]	1800	8.46 ± 1.77	† [16]
32.3	6.32 ± 0.22	[13]	546	8.34 ± 0.36	† [10]
35.2	7.01 ± 0.28	[13]	1800	9.12 ± 0.46	† [10]
38.3	6.08 ± 0.29	[13]			

were calculated taking into account the high-t behavior of the differential cross section. The cross sections of Refs. [12,16] were multiplied by the ratio of the cross section calculated using the $F_1(t)$ form factor in the PPP term to that calculated using the simple exponential form factor. Finally, the cross sections of Refs. [10,11], for which the data are within a limited t-region and have no reliable slope parameters, were calculated as follows: in each case, we evaluated the integrated cross section within the $t-\xi$ region of the experiment using the parameters determined by the experiment, and then recalculated this cross section using the formula of Eq. (3.20), adjusting the normalization parameter D to obtain the same value for the integrated cross section over the same $t-\xi$ region; this formula was then integrated over the region $0<|t|<\infty$ and $1.5/s<\xi<0.05$. The corrections to values derived directly from the published data are of $\mathcal{O}(10\%)$.

In view of the systematic uncertainties in the normalization of the various data sets, as evidenced by the discrepancies among data from different experiments in overlapping s-regions, Fig. 11 shows excellent agreement between the experimental cross sections and the predictions of the one-parameter fit of Eq. (3.20) [using the $F_1(t)$ form factor and $\sigma_0^{\mathbb{P}p}=2.8$ mb].

V. A SCALING LAW IN DIFFRACTION

The renormalization of the Pomeron flux to its integral over all available phase space may be viewed as a scaling law in diffraction, which serves to unitarize the triple-Pomeron amplitude at the expense of factorization.

As mentioned above, an interesting feature of the breakdown of factorization is that the shape of the ξ-distribution of the PPP term is preserved. This is illustrated in Fig. 12, where cross sections are plotted as a function of ξ at fixed t for $\sqrt{s}=14$ and 20 GeV ($\sqrt{s_1}=17$ GeV) and $\sqrt{s_2}=1800$ GeV. As noted by CDF [10], it is seen that the shapes of the $d\sigma/d\xi$ distributions as ξ decreases tend to the shape expected from triple Pomeron dominance at both energies; however, the normalization of the s_2 points is approximately a factor of $(s_2/\overline{s_1})^{\epsilon}=2.6$ lower than that of the $\overline{s_1}$ points, instead of being a factor of $(s_2/\overline{s_1})^{\epsilon}$ higher, as one would expect from factorization [see factor $s'=s\xi$ in Eq. (1.3)].

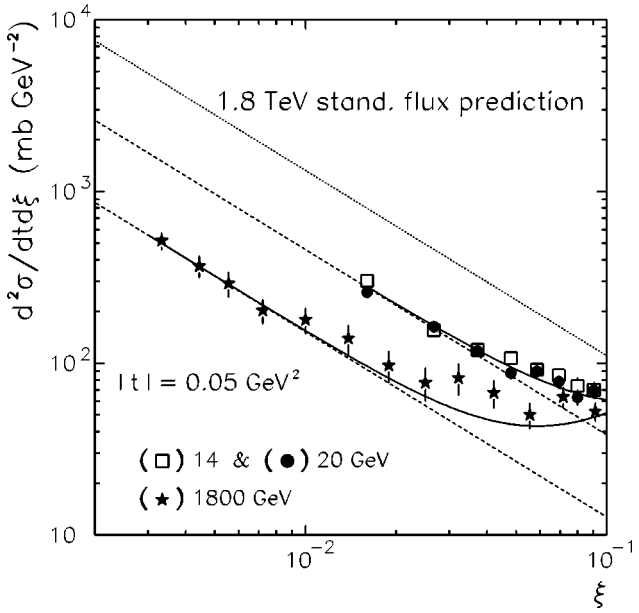

FIG. 12. Cross sections $d^2\sigma_{sd}/d\xi dt$ for $p+p(\bar{p})\to p(\bar{p})+X$ at $t=-0.05$ GeV^2 and $\sqrt{s}=14$, 20 and 1800 GeV. The solid lines are the global one-parameter fit to the data presented in Fig. 9, and the dashed lines represent the renormalized triple-Pomeron contribution. The dotted line is the standard flux triple-Pomeron contribution at $\sqrt{s}=1800$ GeV predicted from the data at $\sqrt{s}=14$ and 20 GeV.

This particular way in which factorization breaks down implies that the $d^2\sigma/dM_X^2dt|_{t=0}$ distribution is approximately independent of s, and therefore *scales* with s, in contrast to the $s^{2\epsilon}$ behavior expected from factorization. Figure 13 shows the differential cross sections as a function of M_X^2 at $t=-0.05$ GeV^2 for $\sqrt{s}=14$, 20, 546 and 1800 GeV within ξ regions not including the resonance region of $M_X^2<5$ GeV^2 (for $\sqrt{s}=14$ and 20 GeV) and not affected by the detector resolution ($\xi>0.005$ and $\xi>0.003$ for $\sqrt{s}=546$ and 1800 GeV, respectively). These cross sections are also shown in Fig. 14 for regions of ξ low enough not to be affected by the non-Pomeron contribution ($\xi<0.03$). In this figure, the data are compared with a straight line fit of the form $d\sigma/dM_X^2\sim 1/M_X^{1+\Delta}$, (solid line) and with the *standard flux* predictions, which are based on factorization (dashed lines). Clearly, factorization breaks down in favor of a scaling behavior.

The scaling of the M_X^2 distribution is a consequence of the Pomeron flux renormalization hypothesis, as pointed out in Sec. III B 1. Figure 6 shows that the renormalization factor based on flux scaling has an approximate $s^{2\epsilon}$ dependence, which cancels the $s^{2\epsilon}$ dependence in $d\sigma/dM_X^2$ expected from

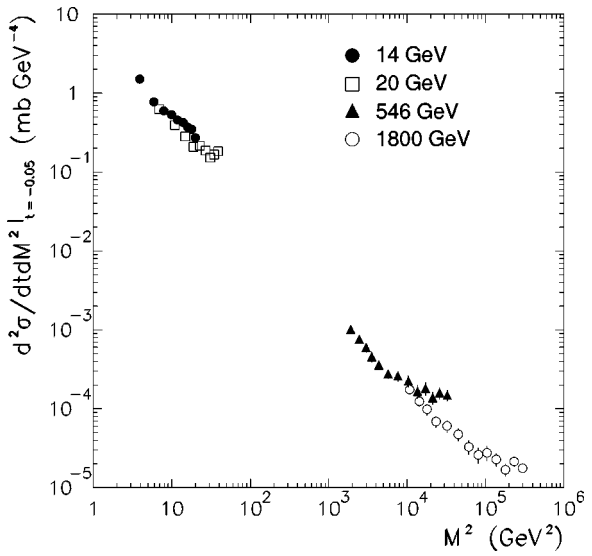

FIG. 13. Cross sections $d^2\sigma_{sd}/dM^2dt$ for $p+p(\bar{p})\to p(\bar{p})+X$ at $t=-0.05$ GeV^2 and $\sqrt{s}=14$, 20, 546 and 1800 GeV.

factorization. An exact comparison between data and theory is made in Fig. 15, where data and predictions of Eq. (3.20) are shown for $t=0$. The $t=0$ data were obtained from the $t=-0.05$ GeV^2 data shown in Fig. 13 by subtracting the pion exchange contribution at $t=-0.05$ GeV^2 and calculating the $t=0$ cross section assuming a t-distribution given by $F_1^2(t)e^{(-2\alpha'\ln\xi)t}$. The excellent agreement between data and theory over six orders of magnitude suggests viewing the Pomeron flux renormalization hypothesis as *a scaling law in diffraction.*

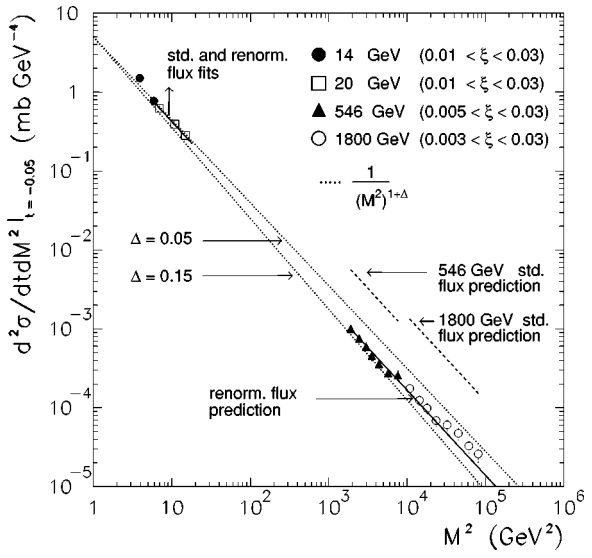

FIG. 14. Cross sections $d^2\sigma_{sd}/dM^2dt$ for $p+p(\bar{p})\to p(\bar{p})+X$ at $t=-0.05$ GeV^2 and $\sqrt{s}=14$, 20, 546 and 1800 GeV. At $\sqrt{s}=14$ and 20 GeV, the fits using the standard and renormalized fluxes coincide; at the higher energies, the standard (renormalized) flux predictions are shown by the dashed (solid) lines.

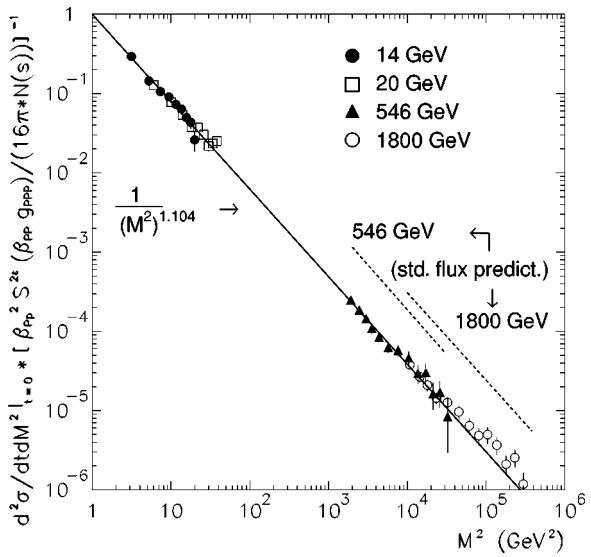

FIG. 15. Cross sections $d^2\sigma_{sd}/dM^2dt$ for $p+p(\bar{p})\to p(\bar{p})+X$ at $t=0$ and $\sqrt{s}=14$, 20, 546 and 1800 GeV, multiplied by $[\beta_{Ppp}^2 s^{2\epsilon}(\beta_{Ppp}\cdot g_{PPP})/(16\pi N(s))]^{-1}$, where $N(s)$ is the integral of the Pomeron flux, are compared with the renormalized flux prediction of $1/(M^2)^{1+\epsilon}$. The dashed curves show the standard flux predictions. The $t=0$ data were obtained by extrapolation from their $t=-0.05$ GeV^2 values after subtracting the pion exchange contribution.

VI. CONCLUSIONS

We have shown that experimental data on diffractive differential cross sections $d^2\sigma/d\xi dt$ for $pp\to Xp$ and $\bar{p}p\to Xp$ at energies from $\sqrt{s}=14$ to 1800 GeV, as well as total diffractive cross sections (integrated over ξ and t), are described well by a renormalized triple-Pomeron amplitude and a Reggeized pion exchange contribution, whose normalization is kept fixed at the value determined from $pp\to Xn$.

The renormalization of the triple-Pomeron amplitude consists in dividing the Pomeron flux of the standard Regge-theory amplitude by its integral over all available phase space in ξ and t. Such a division provides an unambiguous normalization of the Pomeron flux, since the energy scale factor, s_0, which is implicit in the definition of the Pomeron proton coupling $\beta_{Ppp}(0)$ that determines the normalization for the standard flux, drops out. Thus, the renormalized Pomeron flux depends *only* on the value of ξ_{min} and on the Pomeron trajectory, which is obtained from fits to elastic and total cross sections. Therefore the only *free* parameter in the renormalized triple-Pomeron contribution to soft diffraction is the triple-Pomeron coupling constant, g_{PPP}. From our fit to the data we obtained the value $g_{PPP}=1.1$ GeV^{-1}.

The scaling of the Pomeron flux to its integral can be viewed as *a scaling law* in diffraction, which unitarizes the diffractive amplitude at the expense of factorization. A spectacular graphical representation of this scaling is provided by the experimental differential $d\sigma/dM_X^2|_{t=0}$ distribution as a function of M_X^2 for energies from $\sqrt{s}=14$ to 1800 GeV. This

distribution shows a clear $\sim 1/(M_X^2)^{1+\epsilon}$ behavior, which is independent of s over six orders of magnitude, in agreement with expectations from the flux renormalization hypothesis and contrary to the $\sim s^{2\epsilon}$ behavior expected from the standard theory based on factorization.

ACKNOWLEDGMENTS

J.M. would like to thank the Brazilian Federal Agency CNPq for financial support and The Rockefeller University for its hospitality.

[1] K. Goulianos, Phys. Rep. **101**, 169 (1983).
[2] A. Donnachie and P. Landshoff, Phys. Lett. B **296**, 227 (1992).
[3] G. Ingelman and P. Schlein, Phys. Lett. **152B**, 256 (1985).
[4] K. Goulianos, Phys. Lett. B **358**, 379 (1995); **363**, 268(E) (1995).
[5] A. Donnachie and P. V. Landshoff, Nucl. Phys. **B303**, 634 (1988).
[6] R. J. M. Covolan, J. Montanha, and K. Goulianos, Phys. Lett. B **389**, 176 (1996).
[7] E. Gotsman, E. M. Levin, and U. Maor, Phys. Rev. D **49**, R4321 (1994).
[8] A. B. Kaidalov, L. A. Ponomarev, and K. A. Ter-Martirosyan, Yad. Fiz. **44**, 722 (1986) [Sov. J. Nucl. Phys. **44**, 468 (1986)].
[9] A. Kaidalov, in *Proceedings of ''Frontiers in Strong Interactions,''* VII$^{\text{th}}$ Blois Workshop on Elastic and Diffractive Scattering, Château de Blois, France, 1995, edited by P. Chiappetta, M. Haguenauer, and J. Trân Thanh Vân (Editions Frontières, Gif-sur-Yvette, France, 1995), pp. 107–115.
[10] CDF Collaboration, F. Abe *et al.*, Phys. Rev. D **50**, 5535 (1994).
[11] R. L. Cool, K. Goulianos, S. L. Segler, H. Sticker, and S. N. White, Phys. Rev. Lett. **47**, 701 (1981).
[12] J. Schamberger *et al.*, Phys. Rev. D **17**, 1268 (1978).
[13] M. G. Albrow *et al.*, Nucl. Phys. **B108**, 1 (1976).
[14] J. C. M. Armitage *et al.*, Nucl. Phys. **B194**, 365 (1982).
[15] D. Bernard *et al.*, Phys. Lett. B **186**, 227 (1987).
[16] E710 Collaboration, N. A. Amos *et al.*, Phys. Lett. B **301**, 313 (1993).
[17] The justification for using this expression for ξ-values down to $\xi_{\min}=(1.4\ \text{GeV}^2)/s$, which include the resonance region of $\xi < \sim (5\ \text{GeV}^2)/s$, is presented in Fig. 22c of [1], reproduced from Fig. 3c of [18]. This figure shows that the t-integrated cross section, which at high M^2 values has a rather flat M^2 dependence, extrapolates smoothly into the low-M^2 resonance region all the way down to $M^2 \approx 2\ \text{GeV}^2$ and then falls gradually to become zero at the pion production threshold. Taking $M^2=1.4$ [10] (or 1.5 [1]) as the minimum value for M^2 and integrating down to this value using the triple-Pomeron formula provides a very good approximation to the *integrated* cross section over the resonance region.
[18] Y. Akimov *et al.*, Phys. Rev. D **14**, 3148 (1976).
[19] Chung-I Tan, ''Diffractive Production at Collider Energies I: Soft Diffraction and Dino's Paradox,'' hep-ph/9706276, 1997.
[20] S. Erhan and P. Schlein, Phys. Lett. B **427**, 389 (1998).
[21] P. D. B. Collins, *An Introduction to Regge Theory and High Energy Physics* (Cambridge University Press, Cambridge, England, 1977).
[22] R. D. Field and G. C. Fox, Nucl. Phys. **B80**, 367 (1974).
[23] Y. Akimov *et al.*, Phys. Rev. Lett. **35**, 766 (1975).
[24] Y. Akimov *et al.*, Phys. Rev. Lett. **39**, 1432 (1977).
[25] K. Goulianos, ''Comments on the Erhan-Schlein model of damping the Pomeron flux at small x-Pomeron,'' hep-ph/9704454, 1997.
[26] CDF Collaboration, F. Abe *et al.*, Phys. Rev. D **50**, 5550 (1994).
[27] P. E. Schlein, Phys. Lett. B **332**, 136 (1994).